

RHESSI Spectral Fits of *Swift* GRBs

Eric C. Bellm^{*,†}, Mark E. Bandstra^{*,†}, Steven E. Boggs^{*,†}, Wojtek Hajdas^{**}, Kevin Hurley^{*}, David M. Smith[‡] and Claudia Wigger^{**}

^{*}*UC Berkeley Space Sciences Laboratory, 7 Gauss Way, Berkeley, CA 94720-7450, USA*

[†]*Department of Physics, UC Berkeley*

^{**}*Paul Scherrer Institute, Villigen PSI, Switzerland*

[‡]*Santa Cruz Institute for Particle Physics, Santa Cruz, CA, USA*

Abstract. One of the challenges of the *Swift* era has been accurately determining E_{peak} for the prompt GRB emission. RHESSI, which is sensitive from 30 keV to 17 MeV, can extend spectral coverage above the *Swift*-BAT bandpass. Using the public *Swift* data, we present results of joint spectral fits for 26 bursts co-observed by RHESSI and *Swift*-BAT through May 2007. We compare these fits to estimates of E_{peak} which rely on BAT data alone. A Bayesian E_{peak} estimator gives better correspondence with our measured results than an estimator relying on correlations with the *Swift* power law indices.

Keywords: gamma-rays: bursts

PACS: 98.70.Rz; 95.85.Pw

GRB PROMPT EMISSION SPECTROSCOPY WITH RHESSI

The Reuven Ramaty High-Energy Solar Spectroscopic Imager (RHESSI) [1] is a dedicated solar observatory. RHESSI's nine germanium detectors are sensitive from 30 keV to 17 MeV, with excellent resolution in energy (1-5 keV) and time (1 binary μ s) [2]. Each of the nine coaxial detectors is electronically segmented into front and rear segments. Because the detectors are unshielded, RHESSI observes emission from astrophysical sources like GRBs with a $\sim 2\pi$ field of view.

We perform Monte Carlo simulations using the MGEANT package [3] to determine RHESSI's response to off-axis sources like GRBs. RHESSI's response varies with off axis angle, so we create responses every 15 degrees. For each response, we simulate monoenergetic photons in 192 logarithmic energy bins ranging from 30 keV – 30 MeV. Since RHESSI's per-detector response also varies during the spacecraft's four second spin period, we bin the annular response in six azimuthal bins and weight these bins by the total burst lightcurve to create the final response.

The RHESSI data are extracted in SSW-IDL. We fit and subtract a time-varying background, allowing for possible periodic modulation with the spin period. We perform spectral fitting in ISIS [4], a forward-fitting package analogous to XSPEC¹, which is extensively programmable and allows computation of rigorous fluence error estimates via exploration of the parameter space.

Energetic charged particles over time have caused radiation damage to RHESSI's

¹ <http://heasarc.gsfc.nasa.gov/docs/xanadu/xspec/>

germanium detectors. This radiation damage causes broadened spectral lines due to hole trapping and a general loss of active volume. In this work, we restrict our analysis to those detectors which do not exhibit signs of radiation damage. At the time of *Swift*'s launch, six RHESSI segments were usable for spectroscopy; by May 2007 only two segments remained undamaged. In November 2007, RHESSI underwent an annealing procedure to reverse the effects of the radiation damage. The anneal restored some lost sensitivity, but analysis of future bursts will require more sophisticated modeling of the remaining effects of radiation damage on RHESSI's spectral response.

RHESSI-BAT JOINT FITS

We attempted simultaneous spectral fitting for all RHESSI-observed GRBs appearing in the first BAT Catalog [5]. Of 46 candidate bursts, 26 had sufficient RHESSI counts for spectral analysis and produced acceptable joint fits. We selected analysis time intervals manually from the RHESSI lightcurve using a S/N criterion. The resulting intervals were usually shorter than those used in the BAT Catalog. We generated BAT spectra and responses for our intervals with the standard analysis procedures.²

Typically, the joint fits did not require a normalization offset between the RHESSI and BAT data. (Of the four bursts that needed an offset for acceptable fitting, one was in a period of highly modulated RHESSI background, and three were after December 2006 when radiation damage was becoming severe.) For the RHESSI data, we generally fit over the full 30 keV-17 MeV energy band. For bursts coming from the rear of RHESSI, we raised the lower energy bound to ~ 60 keV, as the additional passive material of the RHESSI cryostat can influence the low energy data. For GRB 061007, we omitted the RHESSI data above 3 MeV; there were no significant counts above that level, but the residuals showed systematic deviation which biased the fit.

Our results show good correspondence with comparable fits reported by Konus-Wind and Suzaku-WAM, which also are sensitive in the MeV range [e.g., 6, 7, 8, 9, 10]. For 16 of the 26 bursts, the joint RHESSI-BAT best fit found additional model parameters (E_{peak} and/or β) compared to the BAT-only fit.

We report the results of the joint fits in Table 1.

TESTING E_{peak} ESTIMATORS

The peak energy E_{peak} of the prompt GRB spectrum is crucial to determining overall burst energetics, and it plays a key role in several proposed luminosity indicators. The narrow passband of *Swift*-BAT prevents determination of E_{peak} for many bursts. Accordingly, a number of attempts have been made to infer E_{peak} from the BAT data alone. Butler et al. [11] used a Bayesian fit method with priors determined from the BATSE catalog to estimate E_{peak} . Zhang et al. [12] derived an E_{peak} – BAT power law index correlation using hardness ratios (see also [13]). In Figure 1, we compare the

² http://swift.gsfc.nasa.gov/docs/swift/analysis/threads/bat_threads.html

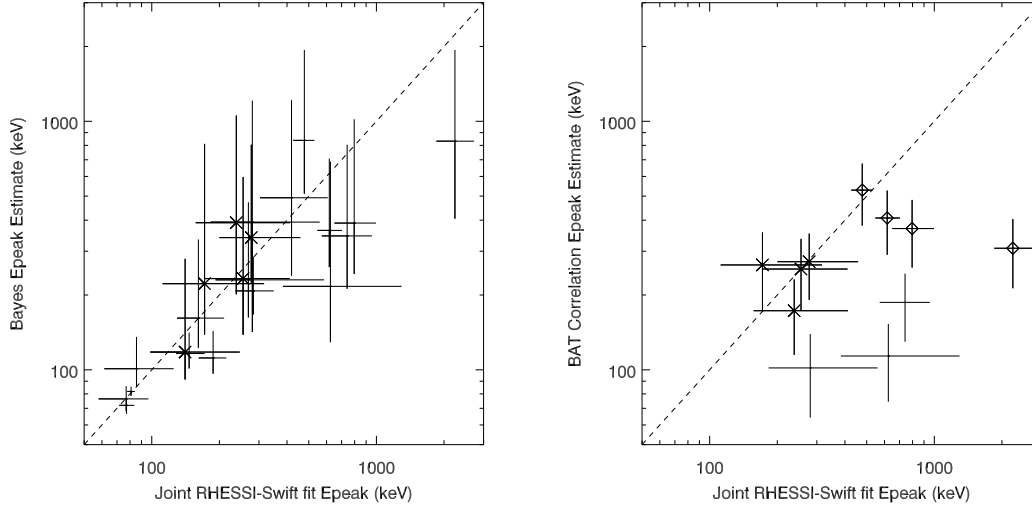


FIGURE 1. Comparison of the measured RHESSI+BAT E_{peak} values with those predicted by [11] (left) and those found with the correlation of [12] (right). Points marked with a cross have fit $\beta > -2$, and hence E_{peak} is only a formal value. Points in the right plot marked with a diamond have BAT-only power law indices outside the range $(-2.3 < \alpha < -1.2)$ likely to yield accurate predictions of E_{peak} [13]. The overplot lines represent equality of the measured and predicted values.

predictions of these models to our joint fit results.

The Bayes model shows good correspondence with the measured values. Above ~ 600 keV, the predicted values of E_{peak} tend to be low, although their error bars reach near the measured values. This deviation is exaggerated somewhat, as our data are for shorter, more intense (and typically harder) burst intervals than used in [11].

Comparison of the Zhang et al. correlation-predicted E_{peak} to our measured RHESSI-*Swift* values shows that this correlation appears to systematically underpredict the measured value of E_{peak} , especially at high energy.

ACKNOWLEDGMENTS

This work was supported by the *Swift* AO-3 GI grant NNX08AE86G.

REFERENCES

1. R. P. Lin et al., *Solar Phys.* **210**, 3–32 (2002).
2. D. M. Smith et al., *Solar Phys.* **210**, 33–60 (2002).
3. S. J. Sturmer, H. Seifert, C. Shrader, and B. J. Teegarden, “MGEANT-A GEANT-Based Multi-Purpose Simulation Package for Gamma-Ray Astronomy Missions,” in *American Institute of Physics Conference Series*, edited by M. L. McConnell, and J. M. Ryan, 2000, vol. 510 of *American Institute of Physics Conference Series*, pp. 814.
4. J. C. Houck, “ISIS: The Interactive Spectral Interpretation System,” in *High Resolution X-ray Spectroscopy with XMM-Newton and Chandra*, edited by G. Branduardi-Raymont, 2002.
5. T. Sakamoto et al., *ArXiv e-prints* **707** (2007), 0707.4626.

TABLE 1. Best joint fit parameters. Spectral models considered are a Band function [14], cutoff power law (CPL), and simple power law (PL). Errors are quoted at the 90% confidence level. Fluence is in the 15 keV–10 MeV band, and analysis times are relative to the BAT trigger time.

GRB	Analysis Interval (sec)	Best Fit Model	α	E_{peak} (keV)	β	Fluence (10^{-6} ergs/cm 2)	χ^2_{ν}
041223	0.0 – 124.0	CPL	$-0.97^{+0.05}_{-0.04}$	$617.^{+86.}_{-70.}$		$87.8^{+8.1}_{-7.1}$	1.21
041224	-3.7 – 36.3	Band	$-0.77^{+0.60}_{-0.32}$	$77.^{+20.}_{-19.}$	$-2.10^{+0.16}_{-0.24}$	$12.9^{+3.8}_{-3.2}$	0.93
050124	-2.2 – 3.8	Band	$-0.65^{+0.72}_{-0.45}$	$86.^{+40.}_{-24.}$	$-2.12^{+0.20}_{-0.50}$	$3.3^{+1.3}_{-1.2}$	0.81
050219B	-29.3 – 10.7	Band	$-1.10^{+0.12}_{-0.10}$	$188.^{+27.}_{-26.}$	$-2.62^{+0.29}_{-0.84}$	$37.1^{+5.1}_{-4.7}$	0.99
050326	-1.1 – 24.9	Band	$-1.01^{+0.13}_{-0.11}$	$277.^{+181.}_{-77.}$	$-1.73^{+0.12}_{-0.19}$	$61.7^{+19.1}_{-16.0}$	0.72
050525A	0.1 – 12.9	Band	$-1.02^{+0.11}_{-0.10}$	$81.^{+3.}_{-3.}$	$-3.12^{+0.25}_{-0.50}$	$21.3^{+1.2}_{-1.1}$	0.90
050713B	-1.6 – 27.4	PL	$-1.40^{+0.04}_{-0.04}$			$43.0^{+4.8}_{-4.7}$	1.03
050717	-0.2 – 35.8	CPL	$-1.13^{+0.04}_{-0.04}$	$2237.^{+483.}_{-386.}$		$65.7^{+7.2}_{-6.9}$	0.92
050802	-3.3 – 22.7	PL	$-1.65^{+0.06}_{-0.07}$			$15.8^{+3.6}_{-3.2}$	1.02
050820B	6.8 – 12.8	CPL	$-0.57^{+0.17}_{-0.16}$	$147.^{+25.}_{-18.}$		$2.6^{+0.3}_{-0.3}$	0.96
051111	-14.5 – 11.5	Band	$-1.04^{+0.19}_{-0.14}$	$255.^{+156.}_{-84.}$	$-1.98^{+0.17}_{-0.46}$	$20.0^{+4.3}_{-4.6}$	0.89
051221A	0.2 – 2.3	Band	$-1.26^{+0.17}_{-0.13}$	$238.^{+175.}_{-81.}$	$-1.98^{+0.11}_{-0.21}$	$4.8^{+0.8}_{-0.8}$	1.35
060110	-0.8 – 11.2	PL	$-1.60^{+0.05}_{-0.05}$			$9.7^{+1.8}_{-1.6}$	0.90
060117	-0.6 – 17.4	CPL	$-1.58^{+0.10}_{-0.09}$	$77.^{+6.}_{-6.}$		$26.8^{+1.4}_{-1.2}$	1.06
060418	-5.2 – 30.8	CPL	$-1.52^{+0.07}_{-0.07}$	$624.^{+671.}_{-240.}$		$22.4^{+7.7}_{-4.4}$	0.92
060421A	-0.3 – 3.7	Band	$-0.88^{+0.33}_{-0.26}$	$141.^{+106.}_{-42.}$	$-1.87^{+0.20}_{-0.63}$	$3.6^{+2.1}_{-1.9}$	0.82
060501	-2.9 – 10.1	PL	$-1.37^{+0.05}_{-0.06}$			$21.9^{+4.5}_{-4.2}$	1.04
060502A	-15.1 – 9.9	Band	$-0.87^{+0.35}_{-0.24}$	$172.^{+144.}_{-60.}$	$-1.98^{+0.26}_{-1.67}$	$11.8^{+7.0}_{-5.9}$	1.04
060614	-1.5 – 3.5	CPL	$-1.56^{+0.12}_{-0.11}$	$280.^{+279.}_{-97.}$		$6.7^{+6.7}_{-1.2}$	0.95
060908	-3.3 – 1.7	CPL	$-0.68^{+0.25}_{-0.20}$	$161.^{+49.}_{-32.}$		$2.0^{+0.4}_{-0.3}$	0.87
061007	-0.8 – 63.2	Band	$-0.85^{+0.04}_{-0.04}$	$478.^{+52.}_{-51.}$	$-2.47^{+0.24}_{-0.42}$	$244.6^{+23.2}_{-22.5}$	0.84
061121	56.0 – 85.0	Band	$-1.31^{+0.04}_{-0.04}$	$741.^{+214.}_{-169.}$	$-2.37^{+0.32}_{-1.21}$	$64.7^{+8.1}_{-8.4}$	1.02
061126	-4.4 – 22.6	CPL	$-1.06^{+0.06}_{-0.05}$	$796.^{+199.}_{-146.}$		$34.0^{+5.3}_{-4.4}$	0.92
061222A	81.9 – 87.9	CPL	$-0.80^{+0.17}_{-0.17}$	$269.^{+316.}_{-77.}$		$7.5^{+6.6}_{-1.8}$	0.91
070220	0.1 – 32.1	CPL	$-1.24^{+0.08}_{-0.07}$	$419.^{+189.}_{-116.}$		$20.3^{+4.9}_{-3.6}$	0.95
070508	2.2 – 18.2	CPL	$-1.07^{+0.07}_{-0.06}$	$283.^{+66.}_{-47.}$		$42.3^{+6.4}_{-4.9}$	0.66

6. H. A. Krimm et al., *ApJ* **648**, 1117–1124 (2006), arXiv:astro-ph/0605507.
7. S. Golenetskii, R. Aptekar, E. Mazets, V. Pal'Shin, D. Frederiks, and T. Cline, *GRB Coordinates Network* **5722**, 1 (2006).
8. K. Yamaoka et al., *GRB Coordinates Network* **5724**, 1 (2006).
9. S. Golenetskii, R. Aptekar, E. Mazets, V. Pal'Shin, D. Frederiks, and T. Cline, *GRB Coordinates Network* **5837**, 1 (2006).
10. K. L. Page et al., *ApJ* **663**, 1125–1138 (2007), arXiv:0704.1609.
11. N. R. Butler, D. Kocevski, J. S. Bloom, and J. L. Curtis, *ApJ* **671**, 656–677 (2007), arXiv:0706.1275.
12. B. Zhang, B.-B. Zhang, E.-W. Liang, N. Gehrels, D. N. Burrows, and P. Mészáros, *ApJL* **655**, L25–L28 (2007), arXiv:astro-ph/0612238.
13. B. Zhang et al., *ApJ* **655**, 989–1001 (2007), arXiv:astro-ph/0610177.
14. D. Band et al., *ApJ* **413**, 281–292 (1993).